The Compact Muon Solenoid Experiment
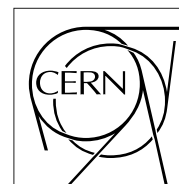
CMS Note

Mailing address: CMS CERN, CH-1211 GENEVA 23, Switzerland

Results from the 1999 Beam Test of a Preshower Prototype

P. Aspell[1], D. Barney[1], P. Bloch[1], J. Bourotte[2], J. Domeniconi[1], A. Elliott-Peisert[1], I. Evangelou[3],
K. Kloukinas[1], A. Kyriakis[4], R. Loos[1], D. Loukas[4], N. Manthos[3], A. Markou[4], J. Mousa[4], F. Peron[1],
S. Reynaud[1], A. Sirunyan[5], E. Tournefier[1], A. Urkinbaev[6], A. Van Hove[1], N. Zamiatine[6]

[1] CERN, Geneva, Switzerland
[2] LPNHE, Ecole Polytechnique, Palaiseau, France
[3] University of Ioannina, Ioannina, Greece
[4] INP, NCSR Demokritos, Athens, Greece
[5] Yerevan Physics Institute, Yerevan, Armenia
[6] JINR, Dubna, Russia

ECAL Group

Abstract

At the end of June 1999 a test of a preshower prototype, equipped with real-size detectors and LHC-style electronics, was tested in the H4 beam at CERN in front of a matrix of "Endcap" crystals. Data were taken with a variety of incident electron energies, and three angles of incidence (to simulate different regions of the CMS endcaps). The prototype functioned well, with a very small startup period and operated successfully for the duration of the test (~ 1 week) without intervention. Good agreement has been found between data and a GEANT-3 based simulation, and the absolute results are promising. Plans are presented for a further test of the prototype in 2000 in the H2 beam inside the 3T magnet.

1 Introduction

1.1 Endcap Supercrystal

In June 1999 a prototype matrix of full size "endcap" ECAL crystals (30mm x 30mm rear face, 22cm long), equipped with VPT readout, was tested in the H4 beam at CERN. The matrix consisted of 5 x 5 full size crystals placed in a carbon fibre alveolar support structure. This "supercrystal" was placed in an environmentally shielded box and placed on the H4 moving table. Tests with high energy electrons were performed. A side view of the box complete with supercrystal is shown in figure 1 below.
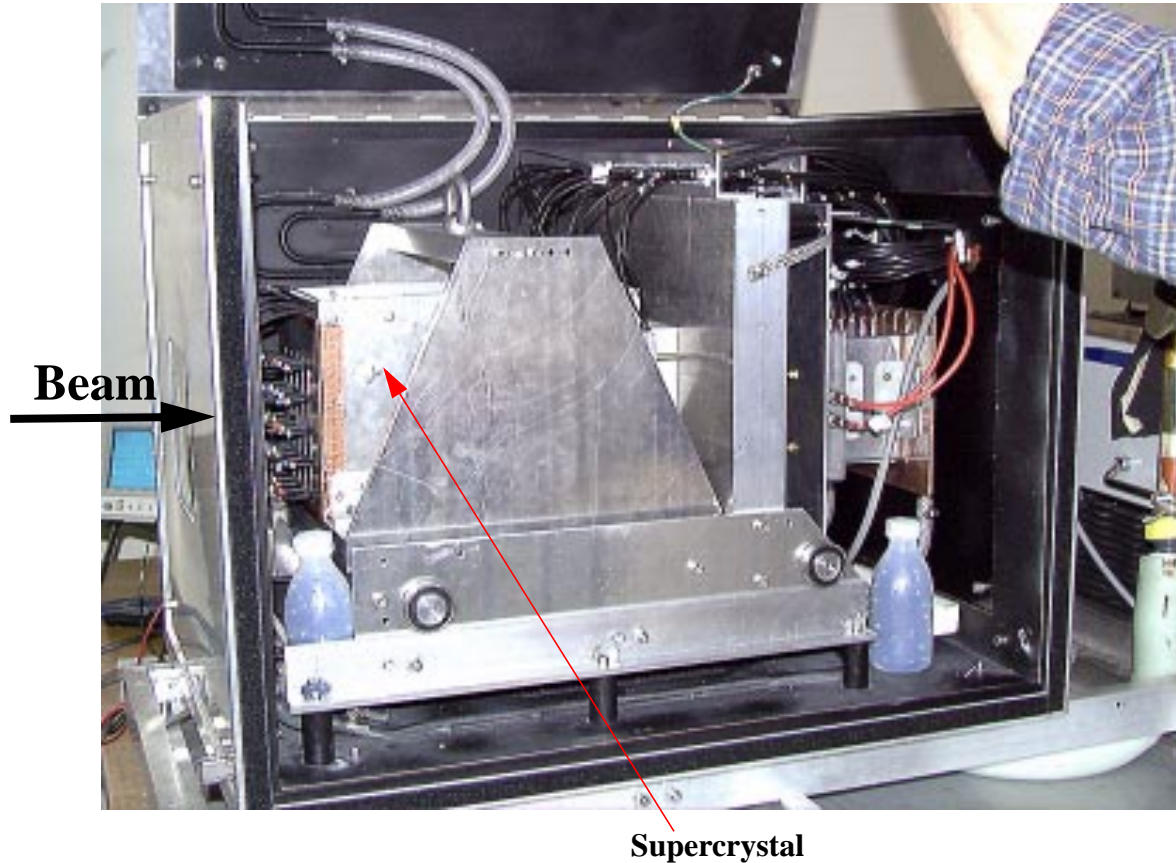

Beam

Supercrystal

Figure 1: Photograph of the Endcap Prototype used in 1999. Note the optic fibres injecting light into the front of the crystals and the "rolling" mechanism that allows the supercrystal to move backwards-forwards within the box.

After one week of tests in H4 a prototype preshower detector was placed upstream of the crystal matrix. For these joint tests the fibres supplying the LED injection signal at the front of the crystals were removed and the supercrystal moved forwards as far as possible.

1.2 Preshower Prototype

The prototype preshower that was installed in the beam in 1999 had previously been tested in 1998 in front of a matrix of barrel-type crystals. Problems with the injection signal into the preshower front-end electronics, coupled with poor APD performance and poor preshower online monitoring resulted in the necessity for a further test in 1999.

The prototype preshower consists of two planes of absorber, constructed from a steel-lead-steel sandwich, each being equipped with an array of 2 x 2 full-sized silicon detectors. The total radiation length in the preshower, as seen by a normally incident particle, was about 3.24 X_0 - see section 1.3. Each silicon detector measured 60 x 60mm^2, with an active area of 57.72 x 57.72mm^2 divided into 32 strips. The detectors were mounted on ceramic

plates which also supported the electronics board containing the front-end ("PACE" [1]) electronics. The ceramic plate was then mounted on a wedge-shaped aluminium tile to form a "micromodule". The wedge allows an overlap of the detectors in one dimension. The array of 2 x 2 micromodules was then placed on a steel support plate. Figures 2 and 3 show, respectively, a single micromodule and one such support plate equipped with its micromodules.
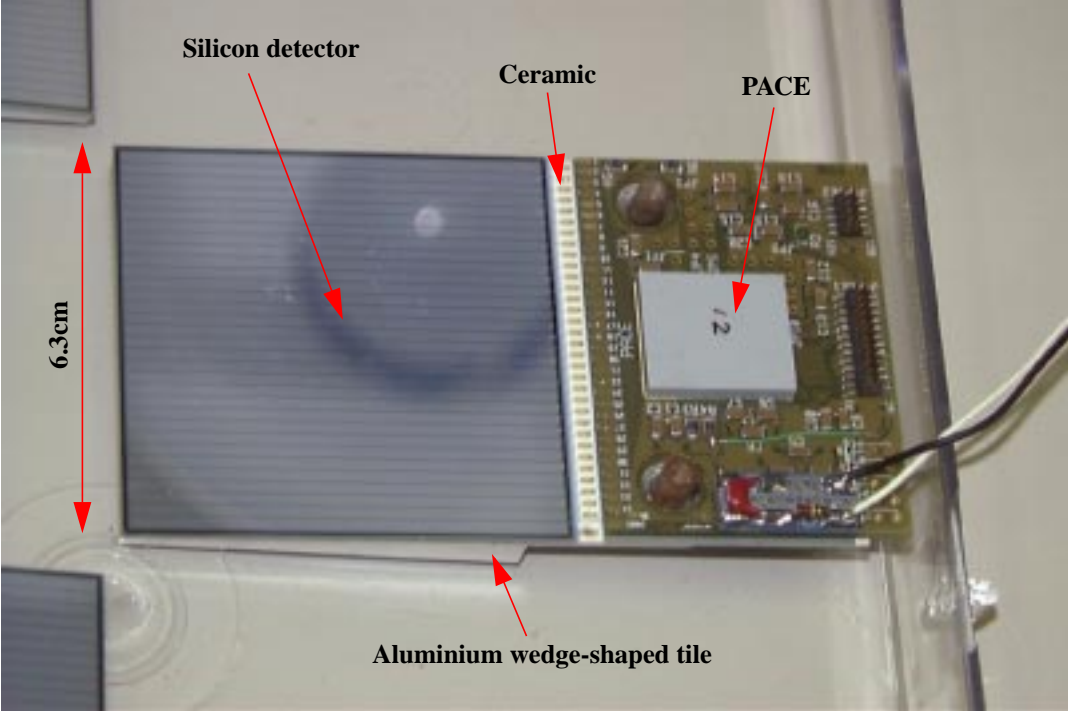

Figure 2: Photograph of a single micromodule as used in the beam tests. The ~2mm-pitch strips on the silicon are evident.
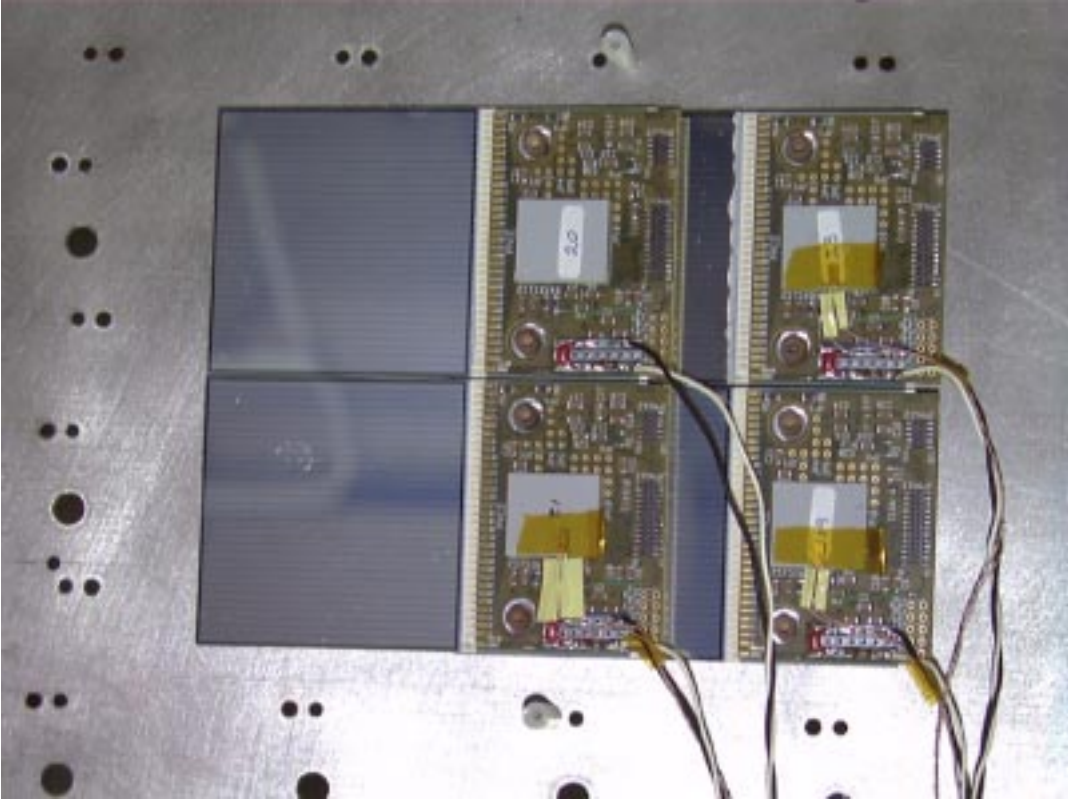

Figure 3: Photograph of a 2 x 2 array of micromodules on a steel support plate. Note the gap between adjacent detectors - parallel to the strip direction.

Each array of detectors has an electronics motherboard placed on top of it. This motherboard contains the control logic for the timing of the system, power distribution and ADCs for each detector. The output from each PACE is connected, via a ribbon cable, to the input of an ADC. A large ribbon cable then routes the digital signals from the motherboard to a dedicated VME module for data acquisition.

Each steel plate has an attached "handle" such that the steel+micromodules+motherboard system is an independent unit which can be easily transported and tested in a standalone way. Two such "macromodules", or simply "planes", are employed in our prototype, each containing 2 x 2 micromodules but having the strips aligned orthogonally. The first plane (most upstream in the beam) has the silicon strips oriented in the vertical direction, and is thus called the "V plane", such that they measure the horizontal coordinate of incident particles, whilst the second plane ("H plane" - closest to the crystals) has horizontal strips.

The two planes are inserted into a mechanical structure which contains cooling planes and layers of absorber material. A top-view of the overall configuration is shown in figure 4.
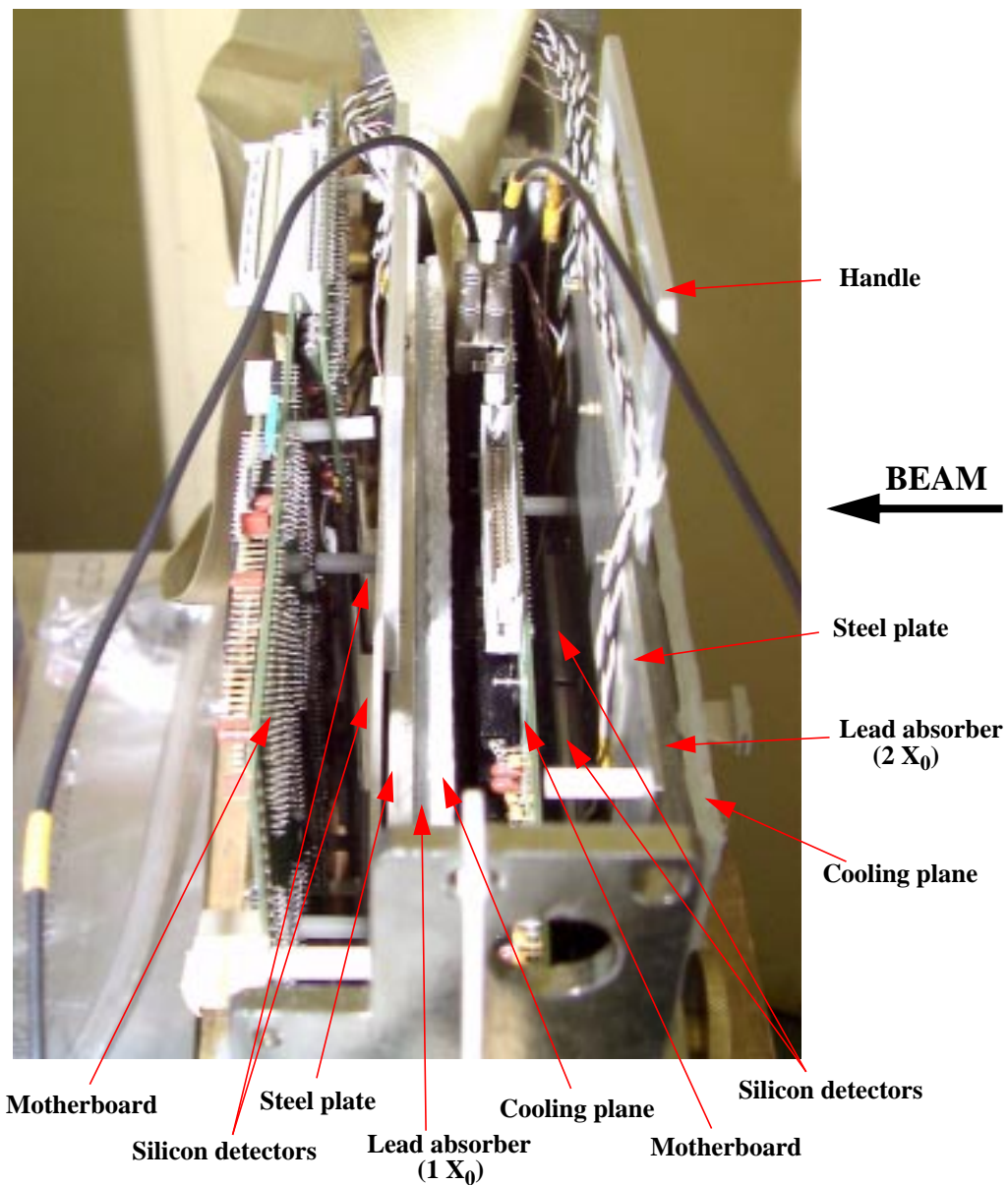

Figure 4: Top view of the preshower prototype, before its environmental shield was placed on top.

The cooling planes are aluminium plates containing embedded serpentines through which water can flow. The cooling planes are in direct contact with the absorber planes such that there is a direct thermal path all the way through to the PACE - one of the major heat sources.

An environmental shield surrounds the complete structure. This is made of copper-coated PCB material. The system is flushed with dry nitrogen which aids cooling, especially of the motherboards which are not in the thermal conduction path from the water-cooled planes. Temperature probes installed in 1998 showed that the temperature inside the box was stable to within 0.1-0.2 degrees, at around 16°C.

The complete preshower system was placed on an aluminium base plate attached to the base plate of the ECAL box. A pivot on one corner of the preshower allowed it to be rotated relative to the crystals (and the beam) by up to 20 degrees, simulating different regions of the endcap. This is shown schematically in figure 5 whilst figure 6 is a photograph of the ECAL + preshower setup installed on the moving table.
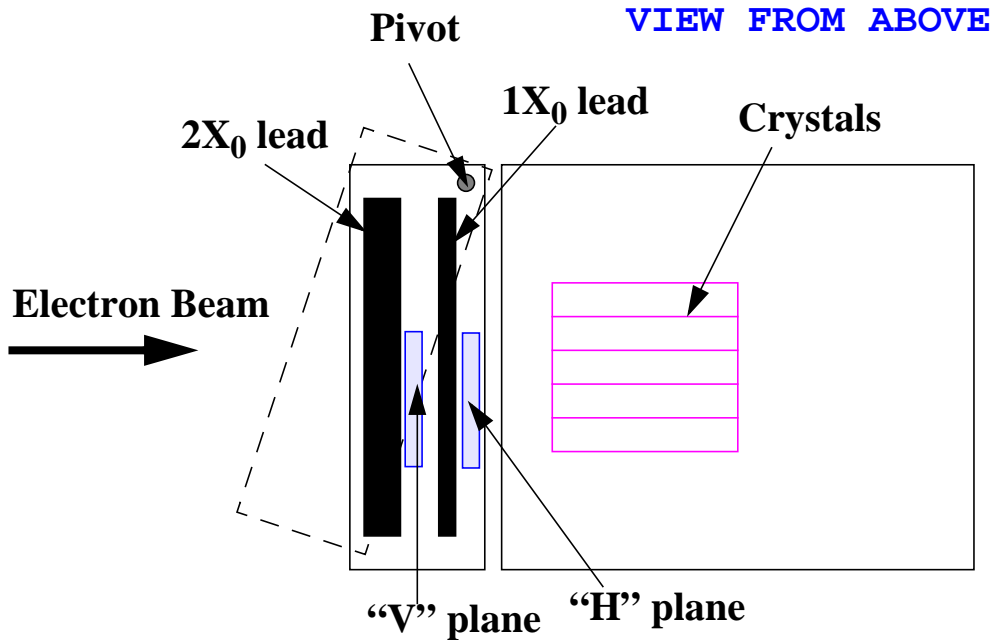

Figure 5: Schematic diagram showing the placement of the preshower relative to the ECAL. The view is from above. Also shown is the pivot system which allows the relative angle between the crystals and preshower to be changed.

Figure 6: Photograph showing the preshower prototype placed in front of the ECAL endcap box. The complete system is situated on the moving table. The beam enters from the right.

The distance between the H-plane detectors and the crystals is about 10cm, 15cm and 20cm for 0, 10 and 20 degree rotations respectively. The range of distance in the real CMS detector is between 10cm (η=2.6) and 14cm (η=1.7).

The preshower was positioned such that the centre of one of the silicon detectors in each plane was essentially colinear with the centre of the central crystal. The numbering scheme for the silicon detectors and crystals is shown in figure 7, which also shows the relative positions of the silicon detectors and crystals..
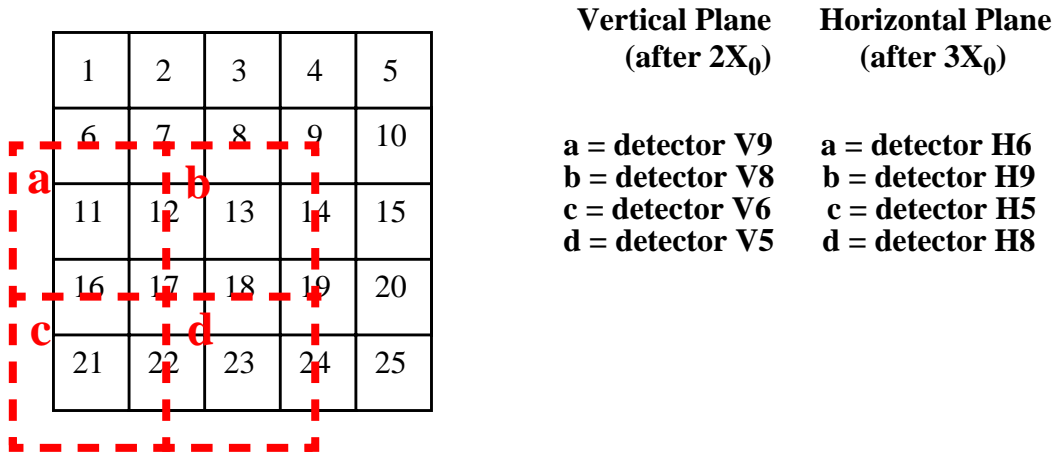

Vertical Plane (after $2X_0$)	**Horizontal Plane** (after $3X_0$)
a = detector V9	a = detector H6
b = detector V8	b = detector H9
c = detector V6	c = detector H5
d = detector V5	d = detector H8

Figure 7: Positioning of the silicon detectors in front of the crystals.

1.3 Simulation Setup

A GEANT-3 simulation of the testbeam has been constructed. It includes the trigger scintillators (which total about 9% of a radiation length), preshower prototype and the endcap matrix. Figures 8 and 9 show, respectively, the overall setup and a close-up of the preshower. The description of the crystal matrix does not include the aluminium pieces placed in front of each crystal; to simulate this a plate of aluminium, 1cm thick, was placed between the preshower and the crystals. Although this plate has little effect on the performance of the ECAL when the preshower is not present, it has a significant effect when it is: after $3X_0$ the shower has developed so many particles deposit energy in this aluminium.
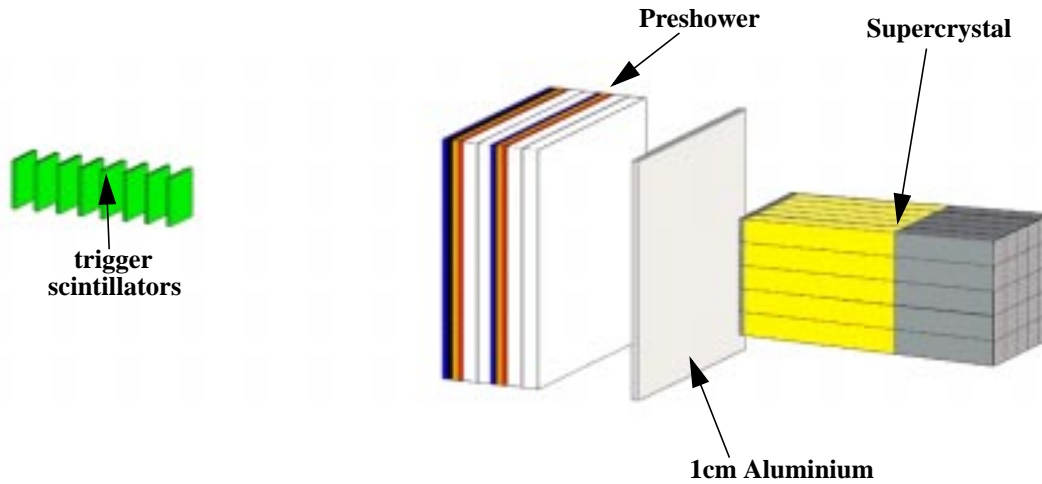

Figure 8: Isometric view of the simulation setup. The beam enters from the left.
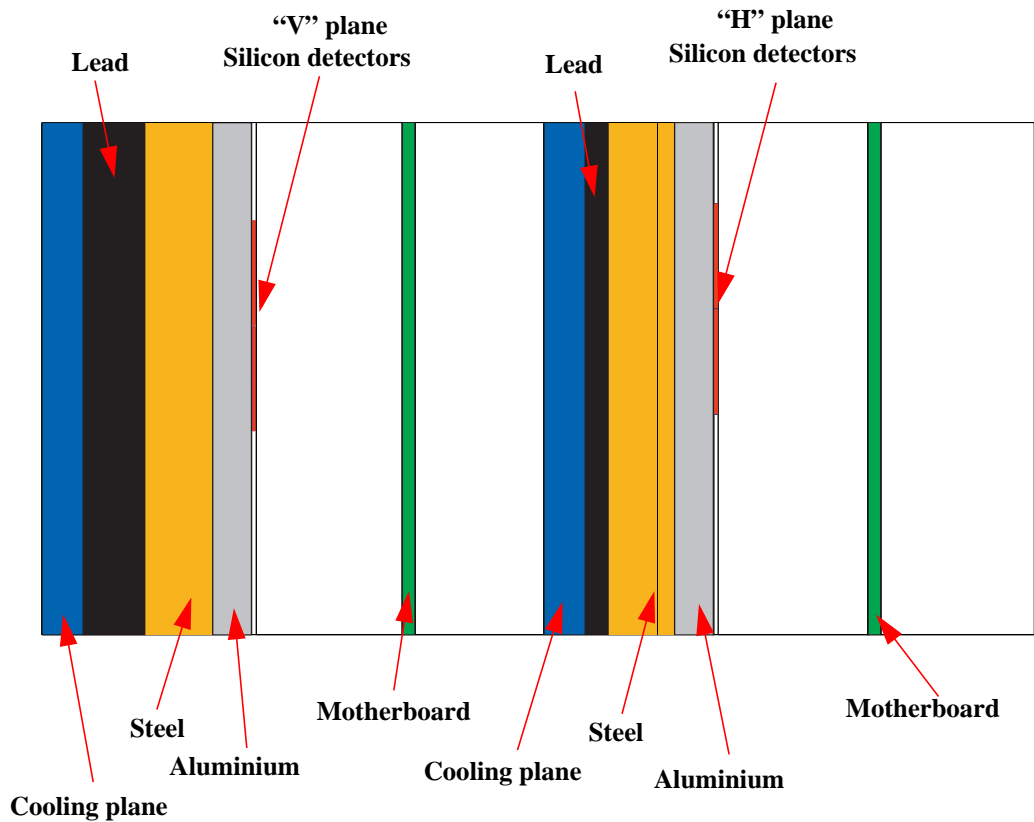

Figure 9: A close-up view of the preshower geometry used in the simulation. The beam enters from the left.

The preshower is described as a simple layered structure, very close to reality. The only real concession to simplicity was the fact that instead of the wedge-shaped aluminium tiles, an average thickness of aluminium was put in, so the silicon detectors are parallel to the absorber plates[a].

The total thickness of the preshower, seen by a normally incident particle, is 3.24 X_0 (2.06 X_0 before the first plane of detectors; a further 1.18 X_0 between the two planes of detectors). This is somewhat higher than the nominal CMS design thickness which at present requires a total of 3 X_0 at $\eta = 1.7$ (equivalent to about 2.7 X_0 for a normally incident particle). The predicted effects of reducing this thickness for further tests in 2000 are presented in section 5.

The simplest test of the validity of the simulation is to run it with and without the preshower and compare the difference in the sum of 9 crystal energy (the calibrated energy seen in a 3x3 matrix of crystals, centered around the crystal with the maximum energy deposit) with that seen in the beam test. This test is independent of any complicated analysis. It was found that this difference was very well modelled when:
- the aluminium plate was in place - between 1.5% (at 15 GeV) and 0.6% (at 180 GeV) of the energy is deposited in this plate.
- the energy cutoffs for photons and electrons were set to 10 keV both in the crystals and all of the preshower materials. The standard GEANT cuts of 1 MeV for CUTGAM and CUTELE were found to be too high - the energy deposited in the sum of 9 was about 1% too high in this case. [b]

It was not found necessary to include delta rays in the simulation so the time penalty incurred by the necessity of the low cutoff energies was not too severe.

---

a. This has very little effect; the thickness of the aluminium wedge varies between about 3.5mm and 6.5mm - the average was set to 5mm. The wedge angle is around 3 degrees.
b. The "standard CMS cuts" of CUTGAM=100keV, CUTELE=1MeV were found to be very good, but this was only discovered after we had already run with 10 keV cuts.

2 Data Taking

2.1 Startup

Emphasis was put this year on a LabView-based online monitoring system. It was included as an add-on to the standard ECAL online monitoring, and fully debugged in the laboratory before being transferred to the beam test. The monitoring system allowed us to view the digital signals coming from a selected ADC (reading the analogue signals from one PACE). The image was updated about once a second, which was adequate for our needs. Figure 10 below shows a screen-dump of the monitoring output. Each ADC outputs 144 digital 12-bit words - four time samples x 36 channels (32 "live" channels + 4 "dummy" channels). Thus the first 36 signals are for the first time sample, signals 37-72 are for the second and so on. The PACE ran at 20 MHz during these tests
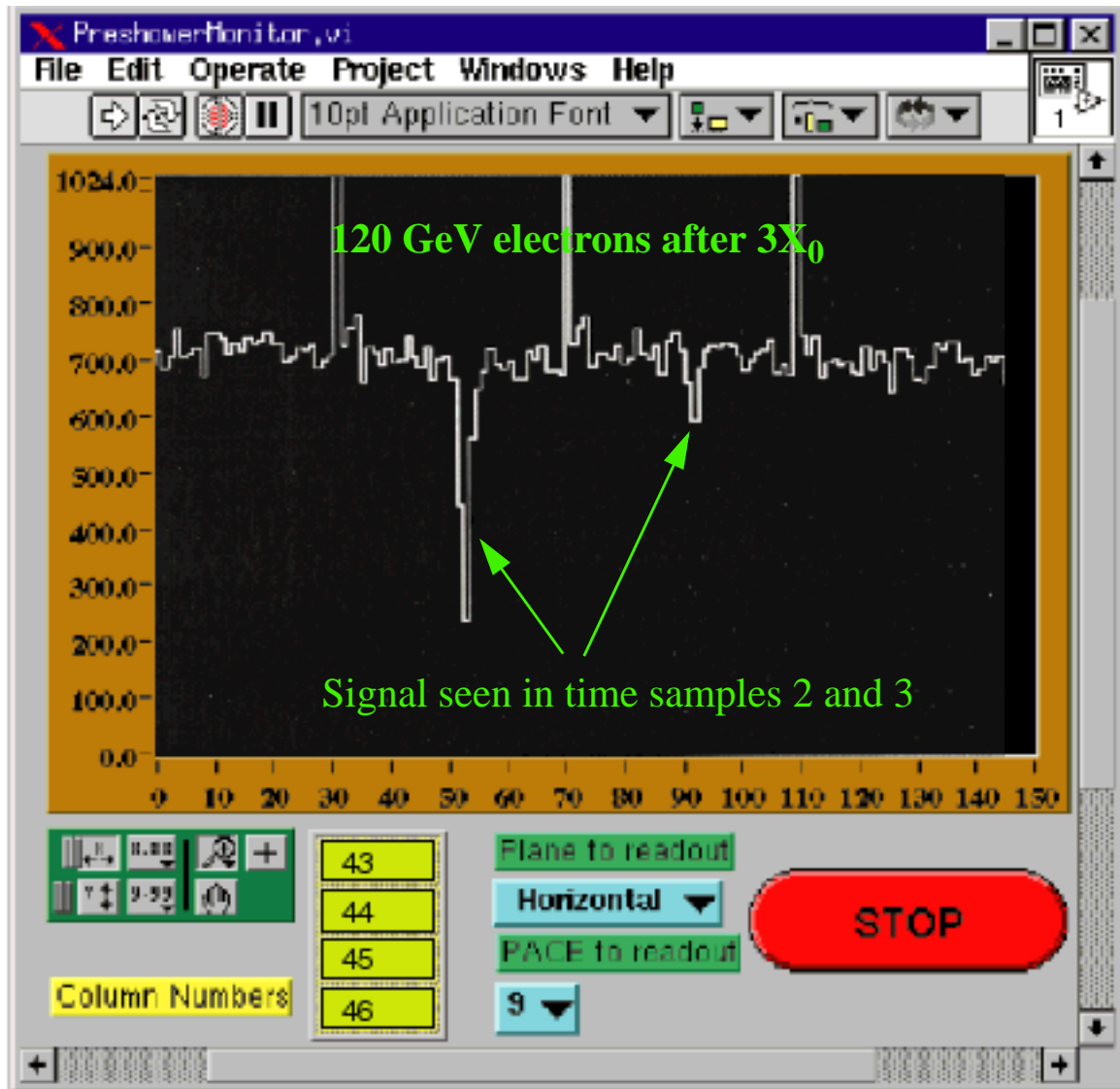

Figure 10: Screen dump of the online monitoring display for the preshower

An additional, and extremely useful, piece of information is the column addresses of the cells which are read-out from the PACE. If these are seen to be non-consecutive it signifies a problem[a]. Unfortunately there are only one set of addresses per plane, so it is impossible to tell if the individual PACE within a plane are synchronized with respect to their addresses. It is envisaged that the column addresses for each PACE will be read-out in CMS.

---

a. This was seen in the laboratory tests when we clocked the PACE at 40 MHz. There is a real, but small, design flaw in the PACE which has been corrected for future implementations. This is the reason why we ran at 20 MHz in these tests.

This monitoring system proved invaluable. To "find" the beam, we simply directed a 120 GeV electron beam at the central crystal, which we had tried to make co-linear with the centre of one of the detectors with our mechanics. We were able to see signals such as those shown figure 10. We could then move the beam around and verify the operation of all the detectors. Installation of the preshower and the verification that we had a working system took only a couple of hours.

With the preshower included in the data acquisition system the maximum number of events that could be taken per burst was a few hundred, to be compared with >2000 for the crystals alone. This meant that we could not realistically perform a complete calibration of the crystals with the preshower included in the DAQ - this would have taken around one day.

2.2 Data Taken

We operated the preshower for a total of 6 days in front of the endcap ECAL prototype. During this time we performed the following functions:
- calibration of the crystals with 50 GeV electrons. The preshower was present physically but it was not included in the data acquisition (due to the time constraints mentioned above) except for the first four runs (see section 3.1).
- Energy scan of the central crystal with the angle between the preshower and ECAL set at zero degrees. The electron energies were: 15, 25, 35, 50, 80, 120 and 180 GeV.
- As above at an angle of 10°
- As above at an angle of 20°
- Position scan of the preshower - 120 GeV electrons incident over different regions to see the effects of gaps between the detector planes.
- Calibration at 120 GeV of the central 3 x 3 crystals. The preshower was again not included in the acquisition.
- The preshower was removed physically from the setup. A calibration at 120 GeV was then performed for all crystals.

3 Data Analysis

3.1 Preshower

In all the energy scan runs the beam was incident on strips 9 to 19 of detector H9 in the second plane. In the first plane the region hit depended on the angle of incidence of the electrons: strips 7 to 19 of detector V8 at zero degrees; strips 16 to 27 of V8 at 10 degrees; strips 30 to 32 of V8 and 1 to 9 of V9 at 20 degrees.

Strip number 14 of detector V8 was dead; therefore only the region from strips 7 to 13 inclusive is used for the analysis at zero degrees. At the beginning of the data-taking period a calibration of the crystals was performed using 50 GeV electrons incident upon each crystal in turn. The first four runs, on crystals 1-4, included the preshower in the DAQ. Figure 7 shows that the preshower detectors were not struck by the beam during these runs so they could be used for preshower pedestal calculation. Pedestals were computed for each channel of each detector.

After pedestal subtraction the noise spectrum in an individual channel in a single time sample has a spread of about 18 ADC counts before common noise subtraction. The noise mainly originates in the PACE and has many contributions: intrinsic pre-amplifier noise, memory non-uniformity, amplification of digital control signals through the substrate. These effects will be much lower (and in some cases non-existent) in the next version of the PACE which will be in DMILL technology and based on Voltage sampling, as opposed to charge integration. The control electronics (digital) and the memory (analogue) will be on separate chips, minimizing the effects of digital crosstalk into the analogue pre-amplifiers.

The common noise is given by the mean of the charge deposited in all channels of the considered detector excluding the following:
- the strip with the highest energy
- its 4 closest neighbours
- channels with more than 40 ADC counts
- dummy channels.

After common noise subtraction the noise decreases to about 8 ADC counts. Variations on this method of common noise subtraction were examined but no significant difference was found.

Since most of the signal is contained in 3 time slots (recall that the PACE stores the signal for 4 consecutive time samples), to optimize the signal-to-noise ratio the energy sum is made over 3 time slots in each plane (samples 2,3 and 4 in plane 1, samples 1,2 and 3 in plane 2)[a].

It was found that the gain as a function of input signal of an individual time sample was not constant. For input signals less than about 50 mips the gain is constant and equivalent to about 6.5 ADC counts per mip. For larger signals, the gain is smaller, as demonstrated in figure 11. After correcting the data for this non-linearity the mean energy deposited in the detector agrees with the simulation to within 10%. The remaining difference is probably due to non-perfect correction of the non-linearity (at high energies) and common-noise (at low energies).

In the data, the number of ADC counts have been converted to Mips by scaling the peak of the distribution so that it is the same as in the simulation. The noise of 8 ADC counts per channel is equivalent to about 2 Mips in the sum of 2 time slots and 4 to 5 Mips on E_i. The long-term aim is to reduce the noise to much less than 1 Mip in the sum of 2 time slots in CMS.

E_i is defined as the sum over 5 strips centered on the most energetic strip for plane i. Figure 12 shows the distribution of E_i for both planes in data and simulation at $E_{beam} = 80$ GeV.

In each plane the particle position is defined as the centre of gravity (weighted by energy) of the 3 strips centered on the most energetic. Only events for which the position measured in the preshower is correlated with that measured in the beam chambers are used in the analysis.

---

a. Although the signal pulse is very fast, the time sampling is asynchronous with the beam, resulting in an effective "jitter" of 50ns.
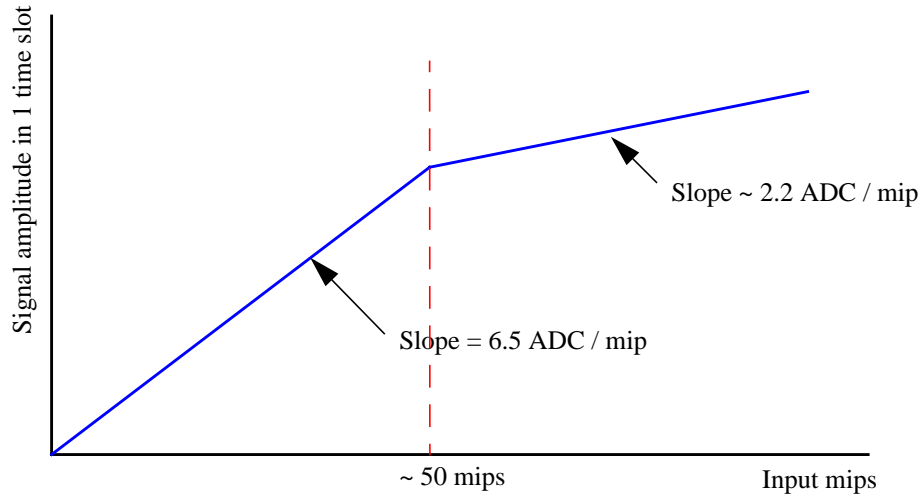
Figure 11: Sketch showing signal amplitude (in ADC counts) in a single timeslot as a function of input signal (in mips).
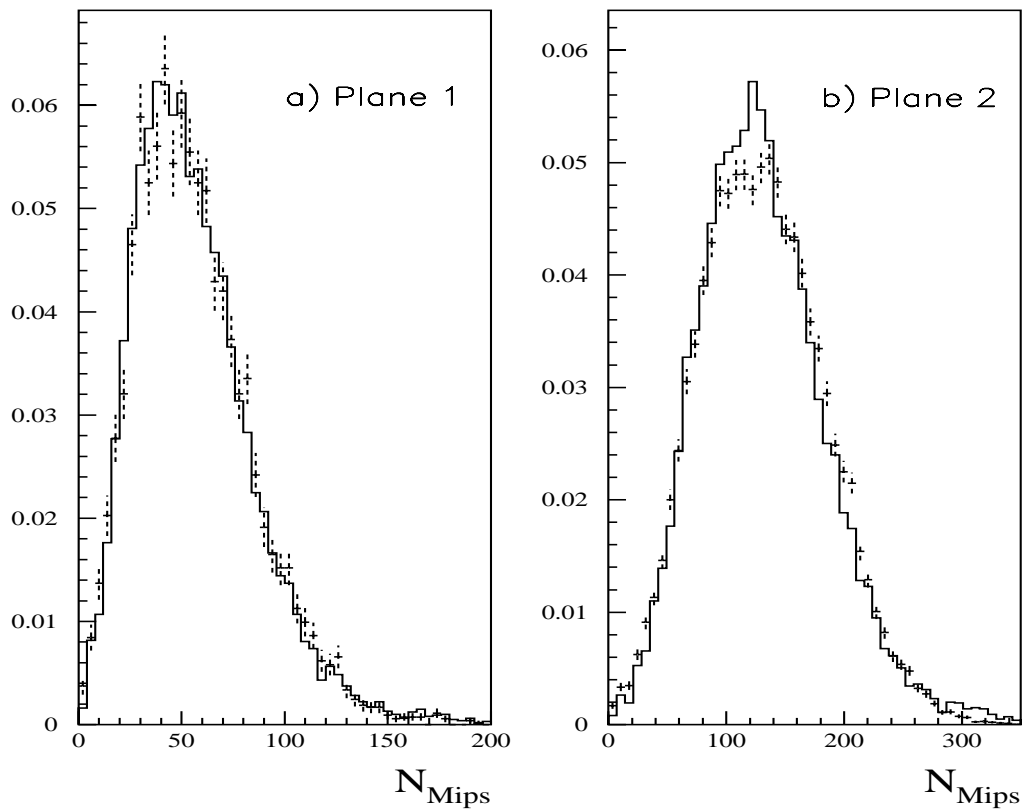

Figure 12: Number of Mips deposited in a) plane 1 and in b) plane 2 for an 80 GeV electron beam. The simulation results are given by the full histograms and the data are the dashed histograms with error bars.

3.2 Crystals

3.2.1 Calibration Coefficients

At the end of the test period a 120 GeV calibration of the crystals was performed using 120 GeV electrons with the preshower in front of the crystals, and then repeated after the preshower had been physically removed. Time constraints meant that we could not perform this calibration for all of the crystals. Table 1 shows a comparison between the inter-crystal calibration coefficients (normalized to the coefficient for crystal 13) found with and without the preshower present.

Crystal	Normalized coefficient with the preshower	Normalized coefficient without the preshower	Difference (%)
7	1.375	1.368	-0.56
8	0.994	0.991	-0.29
9	2.269	2.253	-0.68
10	4.290	4.226	-1.51
12	1.891	1.905	0.75
13	1.	1.	0.
14	2.511	2.487	-0.97
15	1.373	1.373	-0.01
17	1.415	1.439	1.68
18	0.989	0.990	0.10
19	1.641	1.620	-1.32

Table 1: Comparison between inter-crystal calibration coefficients obtained with and without the preshower in place.

The calibration coefficients obtained with and without the preshower are very similar, in most cases differing by less than 1%[a].

The calibration coefficients obtained from runs 28863 and 28887, taken without the preshower in front of the crystals, were used for the following analysis. For the energy scan runs the beam was incident on crystal 13. E_9 (E_{25}) is defined as the sum of the energy deposited in 9 (25) crystals centered on crystal 13.

The noise in the crystals was measured to be 390 MeV for E_9 and 1.1 GeV for E_{25}. These values are somewhat lower than those found during the previous running period of the ECAL alone as the attenuators in the crystal readout chain were changed to give a higher signal/noise ratio.

In the case of 25 crystals the noise is the dominant component in the energy resolution, leading to a big uncertainty on the resolution. This is mainly due to a large coherent component coming from transmission of the signals to the counting room. For this reason we have concentrated our efforts on energy resolution studies with 9 crystals.

The x (y) beam position corresponding to the centre of the crystal is defined as the position for which the mean energy deposited in crystals 12 and 14 (8 and 18), after calibration, is the same. The position of the centre was found to be $x_{beam} = 58.5$mm and $y_{beam} = 60.0$mm. For the energy resolution study the area was restricted to a 4x4 mm^2 square centered on the centre of crystal 13 when possible.

In order to avoid the dead strip at 0 degrees (see section 3.1) the region which was used was displaced by 6mm in x from the centre of the crystal.

---

a. An examination of two calibration runs taken with the ECAL alone shows that for the 16 crystals surrounding the central 3x3 (these crystals are not struck by the beam during energy scans), the mean absolute change in calibration coefficient is around 0.26%.

4 Results

4.1 Energy resolution

4.1.1 Energy resolution of the crystals alone

The energy resolution for the sum of 9 crystals obtained for crystals alone can be parameterized by (excluding the noise contribution):

$$\frac{\sigma_E}{E} = \frac{4.1\%}{\sqrt{E}} \oplus 0.25\%$$

In the simulation, with no noise, it was found to be:

$$\frac{\sigma_E}{E}(\%) = \frac{1.4\%}{\sqrt{E}} \oplus 0.25\%$$

The simulation does not include the photostatistics contribution to the stochastic term. For comparison purposes we added (in quadrature) an extra 3.9% to the simulated stochastic term in the following results, i.e. $3.9\% \oplus 1.4\% = 4.1\%$.

4.1.2 Energy resolution with the preshower

The total energy is defined as

$$E_{tot} = E_9 + E_{presh}$$

where E_9 is the energy (in GeV) in the sum of 9 crystals and

$$E_{presh} = \gamma(E_1 + \alpha E_2)$$

where $E_{1,2}$ are expressed in Mips and γ in GeV per Mip. The dimensionless coefficient α defines the relative weight of both planes and was adjusted in order to obtain the best resolution on E_{tot}. The results are very stable for values of α between 0.6 and 0.8. It was fixed to 0.7 in the following. The value of γ is calculated from the distribution of the mean value of E_9 as a function of $(E_1 + \alpha E_2)$ as shown in Figure 13. Because of the non-linearity for extreme values of $(E_1 + \alpha E_2)$ the value of γ varies slightly with the fitting range. This results in an uncertainty of about 5% on γ. The values obtained for γ are given in table 2 for data and simulation at 0°, 10° and 20°.

In order to compare the energy distributions found in simulation and data, a Gaussian noise of 390 MeV was added to E_9 and a Gaussian noise of 2 Mips was added to each channel of the preshower. Given the values of α and γ the noise in the preshower is equivalent to 160 MeV on E_{tot} which should be added in quadrature to the noise from the crystals.

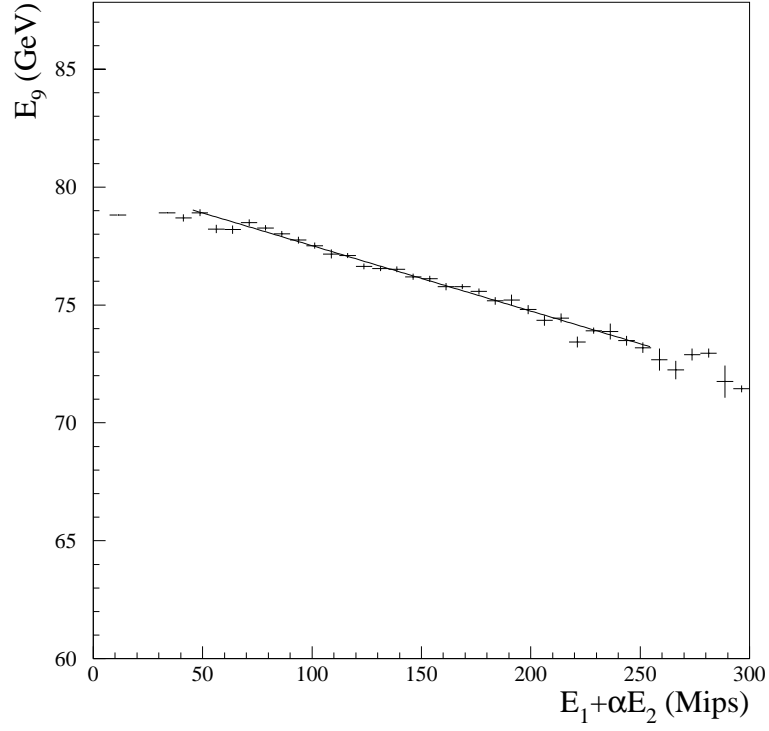**Figure 13:** E_9 versus ($E_1+\alpha E_2$) in the data for E_{beam} =80 GeV. The line is the result of the fit.

	Slope of E_9 vs ($E_1 + \alpha E_2$) (GeV/Mip)					
	0° Incidence		**10° Incidence**		**20° Incidence**	
Energy (GeV)	**Data**	**Simulation**	**Data**	**Simulation**	**Data**	**Simulation**
15	0.026	0.028	0.031	0.028	0.031	0.030
25	0.027	0.027	0.032	0.028	0.031	0.030
35	0.027	0.027	0.030	0.028	0.029	0.029
50	0.027	0.027	0.028	0.027	0.029	0.028
80	0.027	0.025	0.029	0.027	0.027	0.028
120	0.026	0.025	0.027	0.027	0.028	0.028
180	0.023	0.024	0.025	0.026	0.027	0.028

Table 2: Values for the slope of E9 vs (E1+αE2) in GeV/Mip for data and simulation for all angles of incidence.
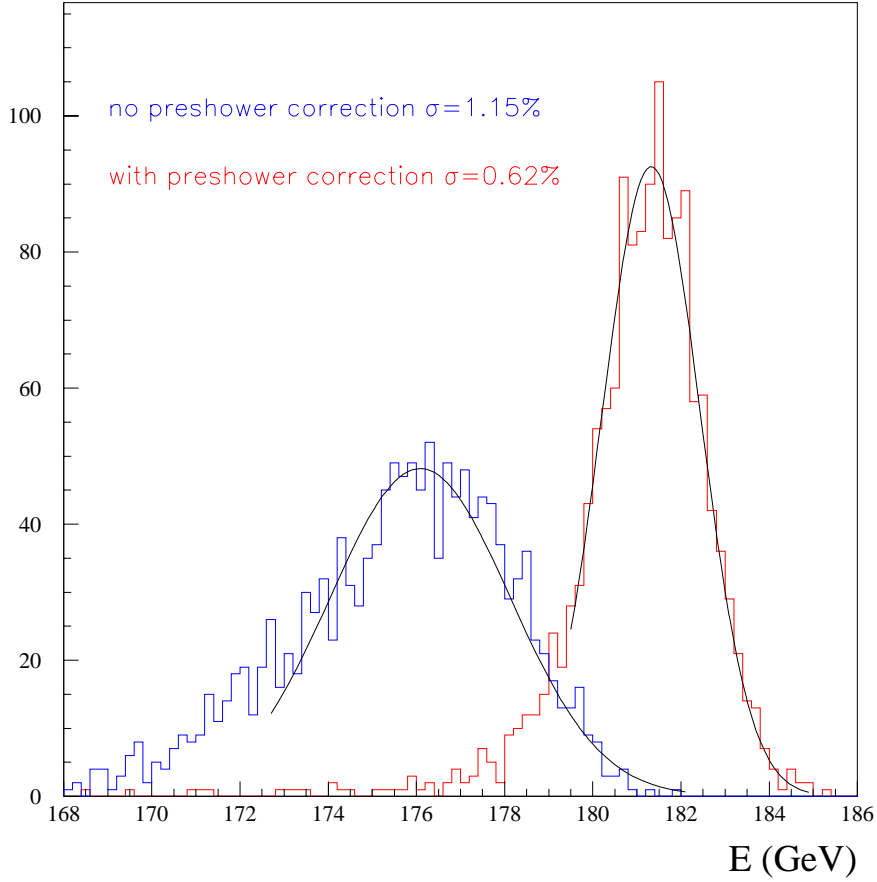
Figure 14: Distribution of E_9 (no preshower correction) and of E_{tot} for E_{beam} = 180 GeV in the data.

Figure 14 shows the distribution of E_9 and E_{tot} for E_{beam} = 180 GeV in the data. Since the spectra do not follow simple Gaussian distributions the energy resolution is obtained from a Gaussian fit on the restricted range from 1.5σ below the mean to 3σ above.

The quadratic difference of the energy resolution obtained in the simulation with and without noise gives the value of the effective noise. Because the distributions are not perfectly Gaussian the effective noise was found to be 10% higher than the standard deviation parameter of the Gaussian random number generator used to inject noise. We took a pragmatic approach such that the noise which is subtracted from the energy resolution is taken as 110% of the measured noise.

The fraction of energy deposited in the preshower is given by $f_E=1-<E_9>/<E_{tot}>$ where $<E_9>$ ($<E_{tot}>$) is the position of the peak of the distribution of E_9 (E_{tot}) . The value of $1-f_E$ (i.e. $<E_9>/<E_{tot}>$) as a function of energy is shown in figures 15 and 16 for zero and 10 degree incidence angles respectively. The simulation agrees well with the data showing that the energy deposition in the preshower is well understood.

The energy resolution before preshower correction (i.e. on E_9) after noise subtraction is shown in Figure 17.

Figures 18, 19 and 20 show the energy resolution after preshower correction (i.e. on E_{tot}) for the 3 incidence angles respectively. The noise is subtracted and a stochastic term of 3.9% (see section 4.1.1) has been added to the energy resolution found in the simulation.
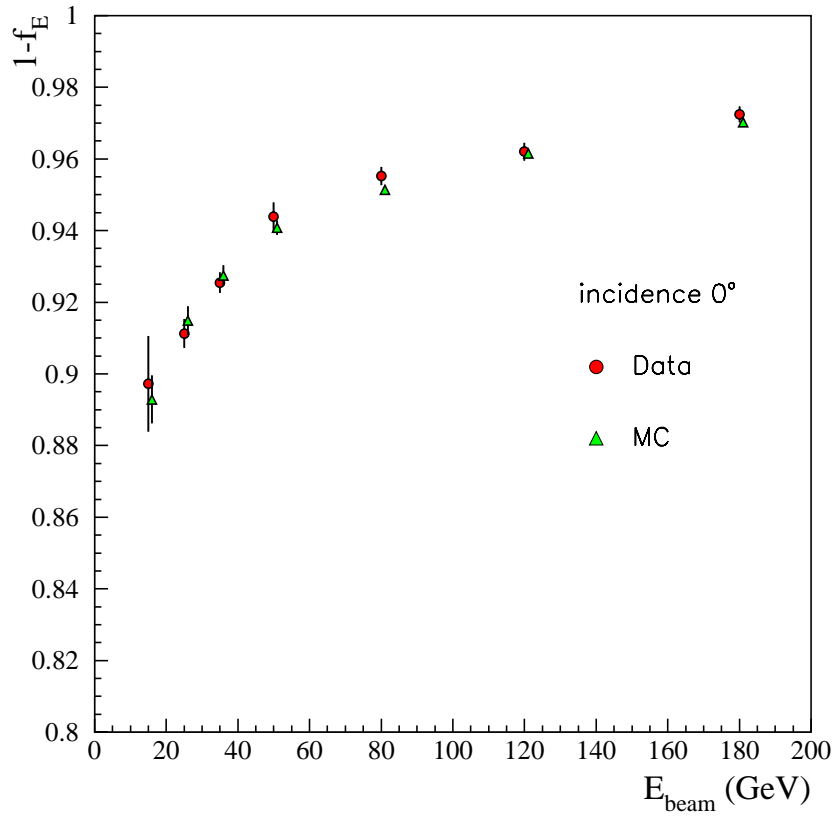
Figure 15: Fraction of energy deposited in the crystals as a function of energy for zero degrees incidence.
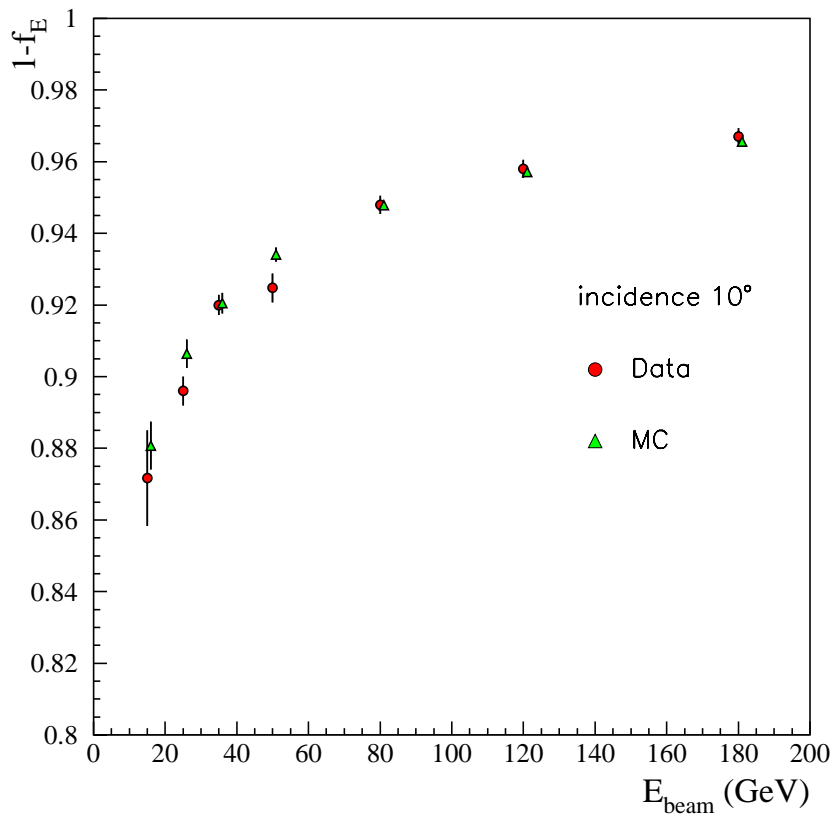

Figure 16: Fraction of energy deposited in the crystals as a function of energy for 10 degrees incidence.
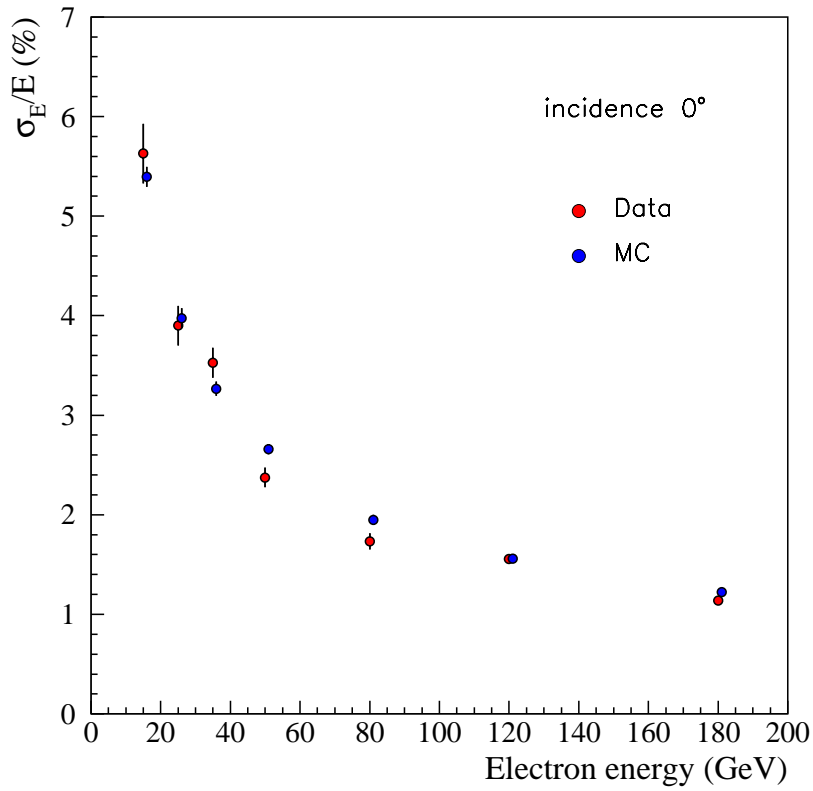
I

Figure 17: Energy resolution before preshower correction. The noise in the crystals and in the preshower is subtracted.
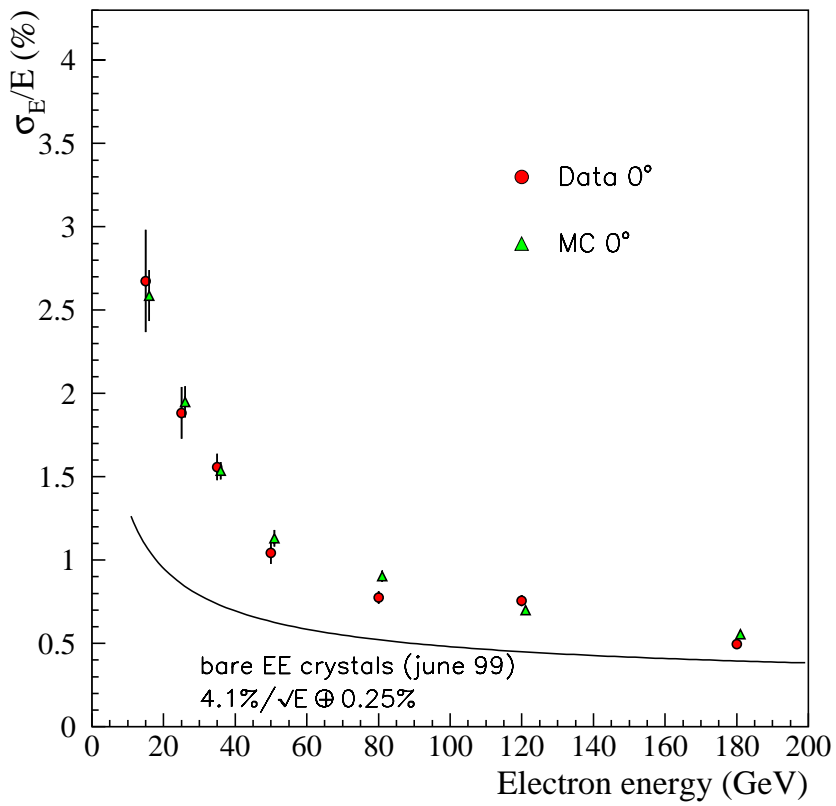

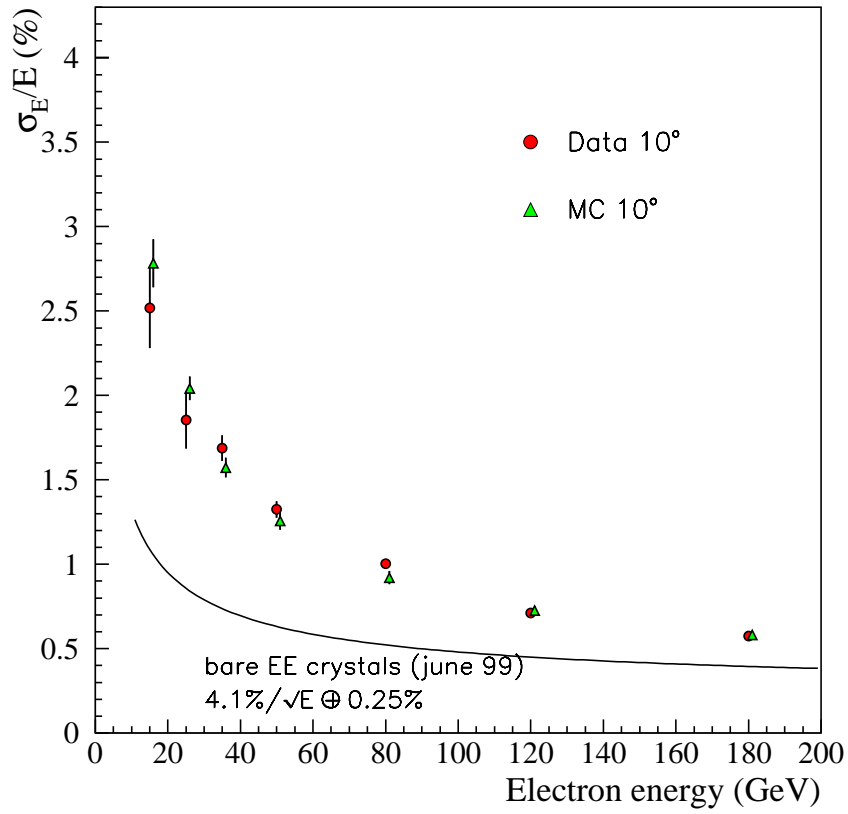**Figure 18:** Energy resolution after noise subtraction for an incidence of zero degrees.

Figure 19: Energy resolution after noise subtraction for an incidence of 10 degrees
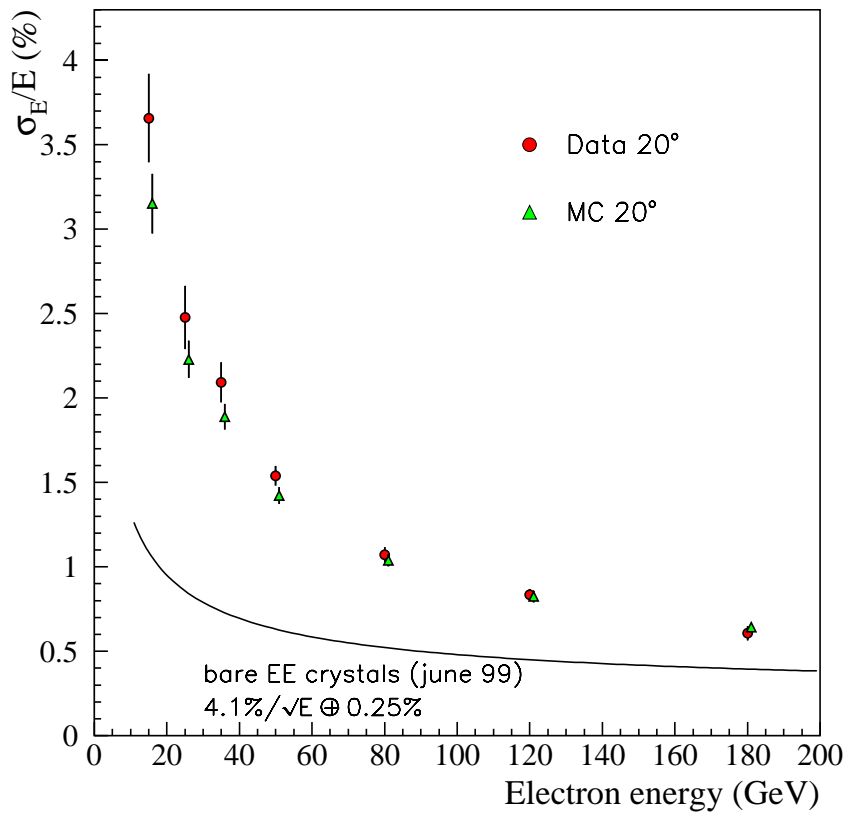
Figure 20: Energy resolution after noise subtraction for an incidence of 20 degrees

The contribution of the preshower to the energy resolution is obtained by subtracting the known resolution of the crystals alone:

$$\frac{\sigma_{\text{Preshower}}}{E_{\text{beam}}} = \sqrt{\left(\frac{\sigma_{\text{tot}}}{E_{\text{beam}}}\right)^2 - \left(\frac{\sigma_{\text{crystals}}}{E_{\text{beam}}}\right)^2}$$

The "preshower term" measured in the simulation is shown in figure 21 for the 3 incidence angles.
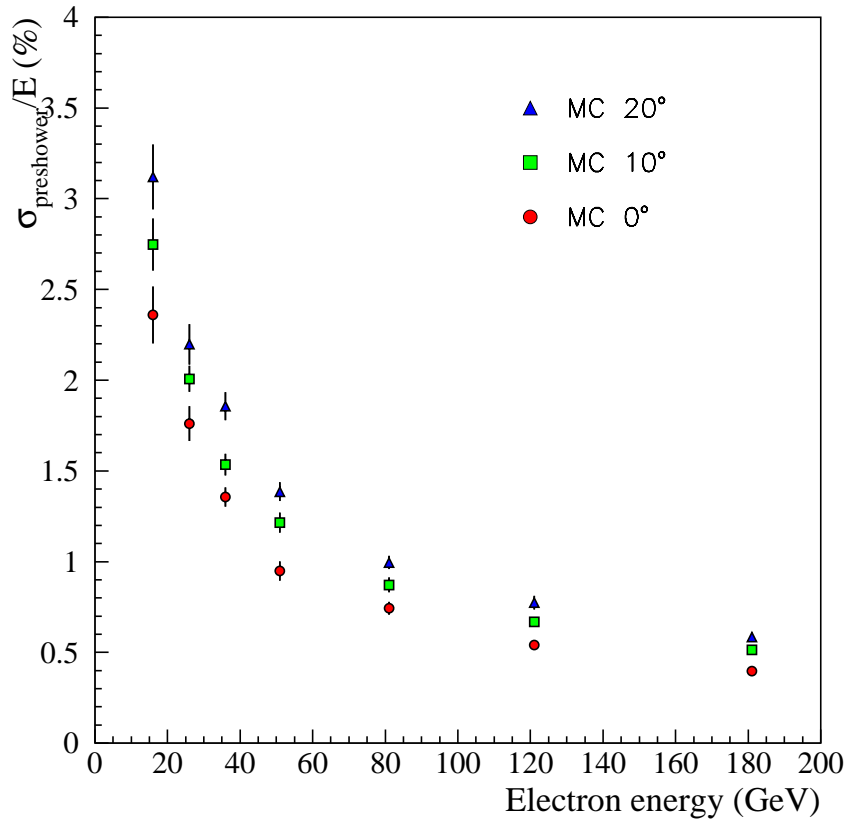
Figure 21: Contribution from the preshower to the energy resolution.

As the angle of incidence increases, the thickness of absorber "seen" by the particle increases accordingly, resulting in a larger amount of energy being deposited in the absorber. Clearly the less energy deposited in the preshower, the better the energy resolution.

4.2 Spatial Precision

An energy-weighted centre-of-gravity method was used to calculate the beam incidence position in the preshower planes ($X_{preshower}$, $Y_{preshower}$), using 3 strips centered on the one with the maximum energy deposit. The reference positions (X_{beam}, Y_{beam}) were defined by wire chambers upstream of the preshower using the method defined in [3]. X_{beam} and Y_{beam} are actually the positions measured by the wire chambers extrapolated to the preshower. The precisions of X_{beam} and Y_{beam} thus depend on the beam energy, and also on the angle of the preshower detectors relative to the beam[a]. The measured uncertainties on X_{beam} and Y_{beam} are given in table 3.

Beam Energy (GeV)	0° Preshower Angle		10° Preshower Angle		20° Preshower Angle	
	$\sigma X_{beam}(\mu m)$	$\sigma Y_{beam}(\mu m)$	$\sigma X_{beam}(\mu m)$	$\sigma Y_{beam}(\mu m)$	$\sigma X_{beam}(\mu m)$	$\sigma Y_{beam}(\mu m)$
180	127	147	135	151	142	158
120	127	163	147	166	143	172
80	151	163	160	185	162	187
50	181	227	189	228	197	240
35	204	249	213	252	219	263
25	224	266	223	270	237	296
15	240	298	238	288	249	315

Table 3: The precision of the extrapolations from the beam chambers.

At high energies a plot of, for example, $Y_{preshower}$-Y_{beam} vs $Y_{preshower}$ shows a characteristic S-curve shape (figure 22a), similar to that seen in the crystals. This is due to the lateral distribution of the shower and can be used to apply a correction to the measurement. The S-curve is not evident at low energies, as can be seen in Figure 22b.
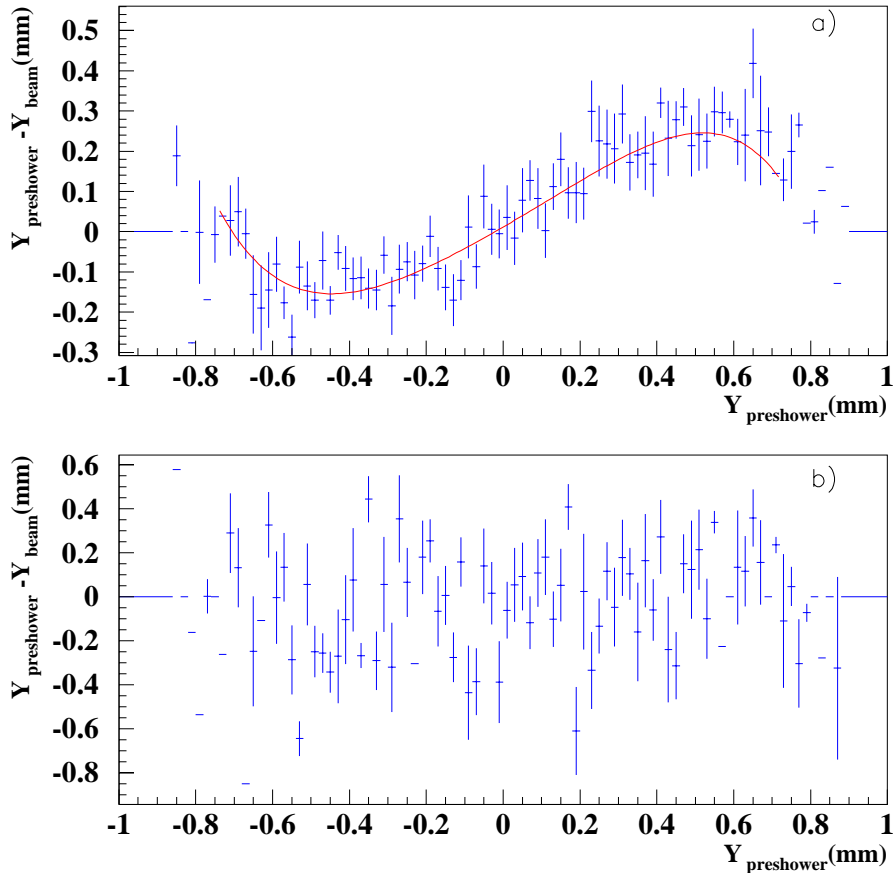

Figure 22: S-curve characteristic shape in the second plane for a) 180 GeV electrons, b) 15 GeV electrons.

---

a. To compare the positions measured by the preshower and the beam chambers we have to convert to the same coordinate system - which in this case is the internal coordinate system of the preshower silicon detectors.

The improvement the S-curve correction makes at high energy is evident in figures 23 and 24 which show the spatial precision in the preshower planes for 180 GeV electrons (before subtracting the error on the beam chambers) before and after S-curve correction respectively.

Figures 25-30 show the spatial precisions measured for the preshower planes as a function of incident electron energy for each of the three incidence angles after S-curve correction. For the second plane there is a good agreement between data and simulation, but it is not so good for the first plane. It should be noted that noise has not been included in the simulation in these plots. If 2 Mips noise is included, as was done for the energy resolution, the simulation results get slightly worse, especially at low energies, and the agreement for the first plane improves. However, the agreement for the second plane degrades. Uncertainties on the level of noise in the preshower, and differences between the S-curve corrections in data and simulation are probably responsible for these discrepancies. It is worth pointing out that in any case the spatial precision is always better than 500μm.

There is a slight improvement in precision as the angle of incidence increases, due to the thicker amount of absorber traversed (resulting in a larger lateral shower development).
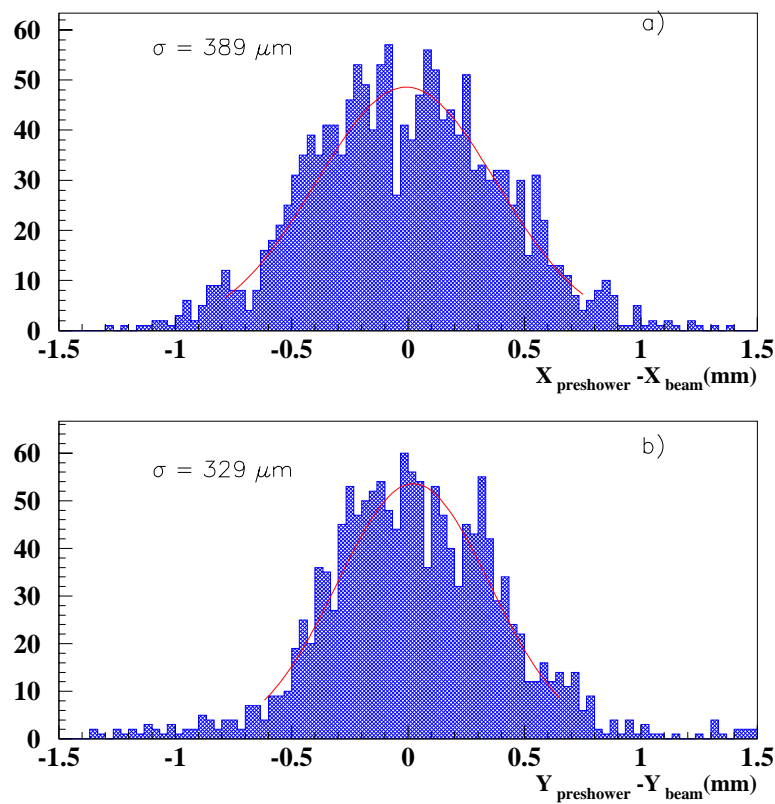

Figure 23: Spatial precision of the two preshower planes, before S-curve correction, for 180 GeV electrons at zero degrees incidence angle.
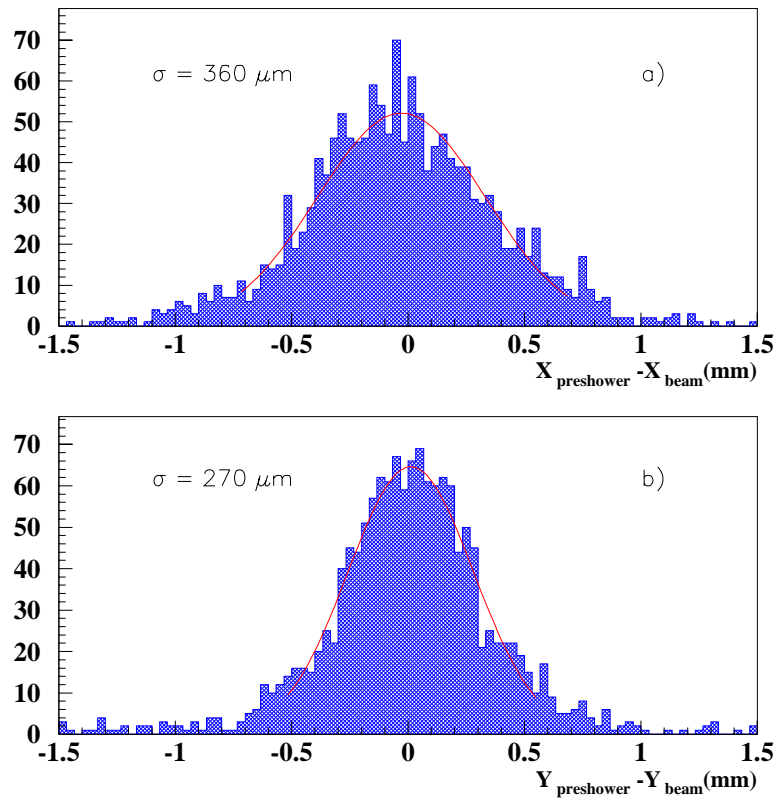
Figure 24: Spatial precision of the two preshower planes, after S-curve correction, for 180 GeV electrons at zero degrees incidence angle.
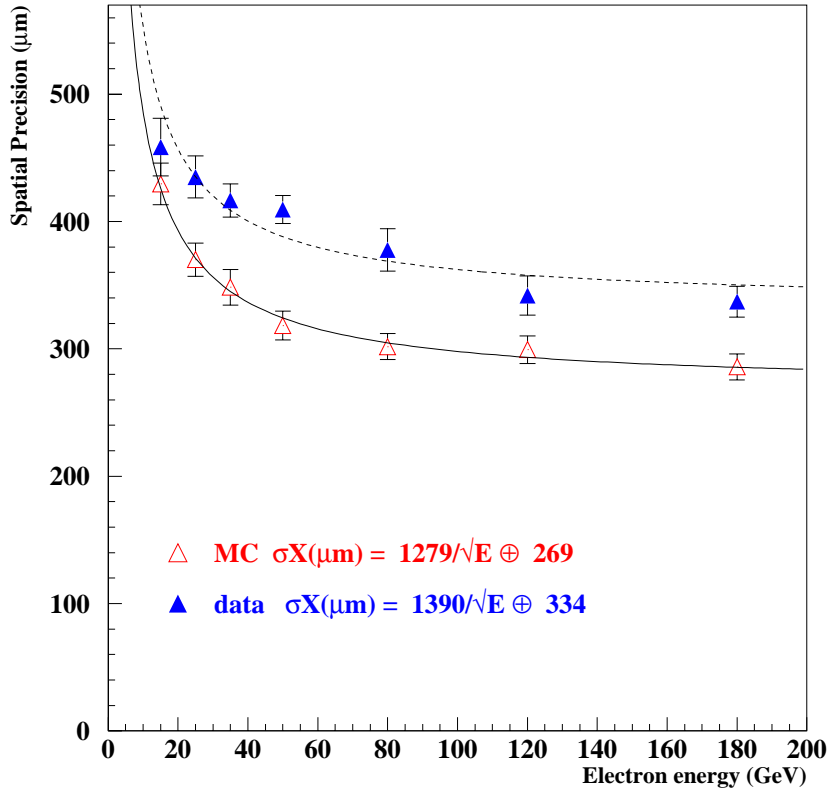
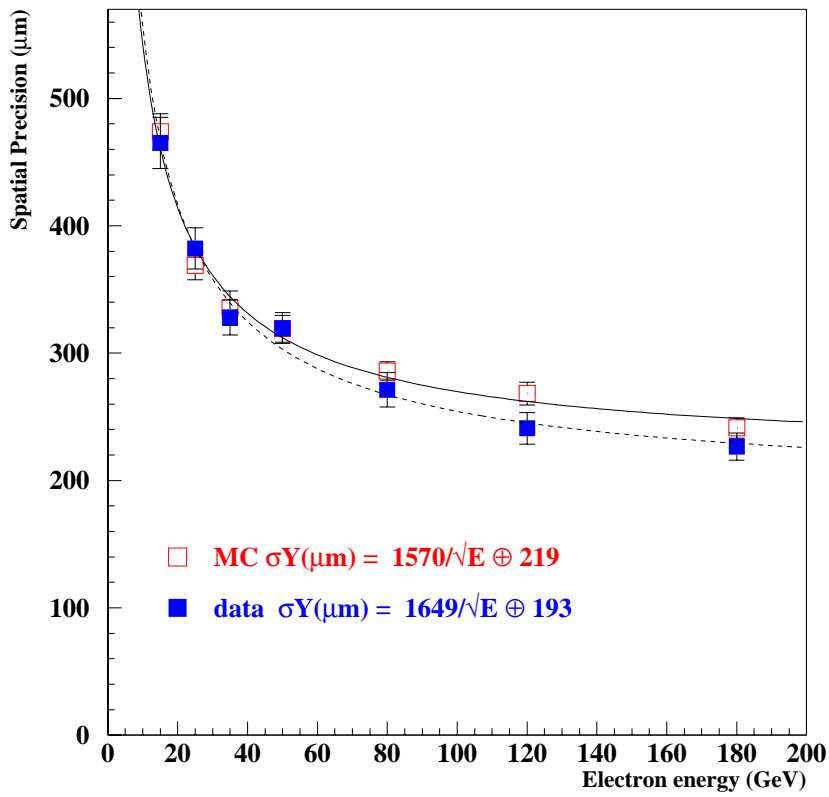**Figure 25:** Spatial precision as a function of electron energy for the first plane, zero degrees incidence angle.

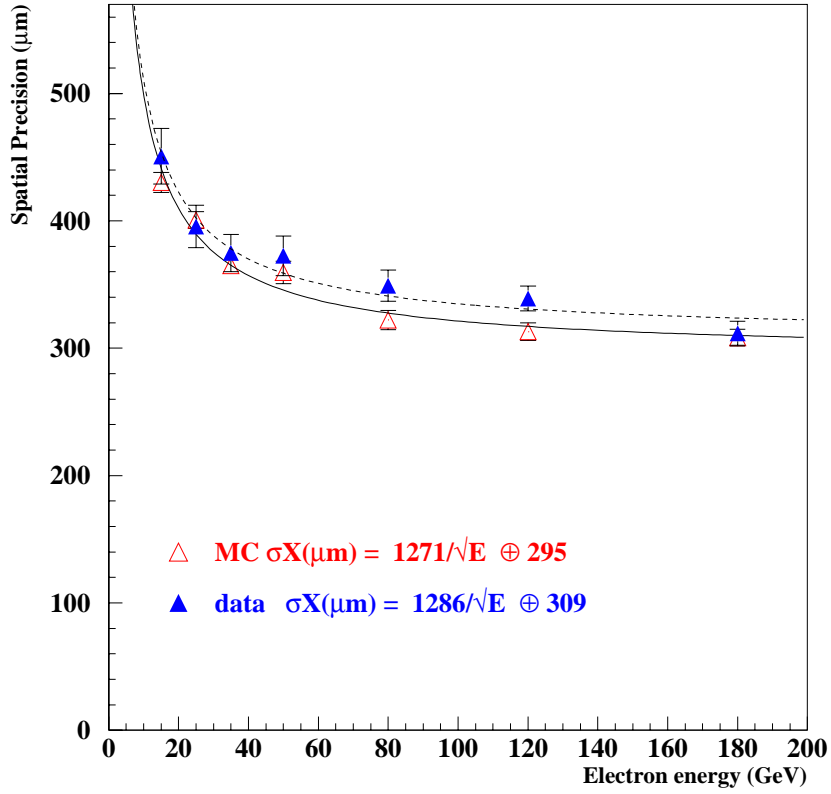**Figure 26:** Spatial precision as a function of electron energy for the second plane, zero degrees incidence angle.

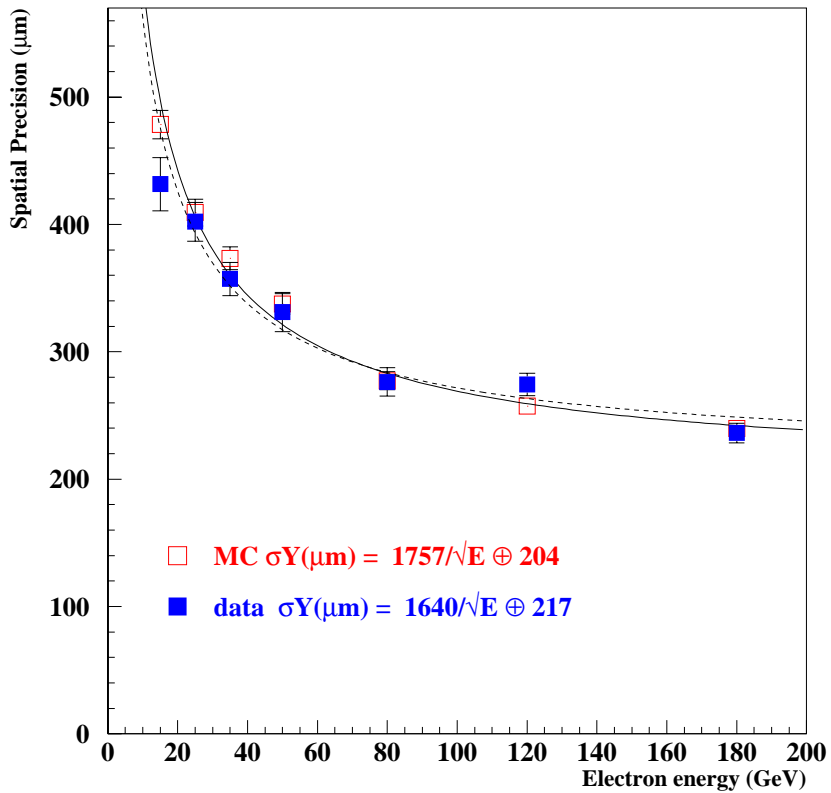**Figure 27:** Spatial precision as a function of electron energy for the first plane, ten degrees incidence angle.

Figure 28: Spatial precision as a function of electron energy for the second plane, ten degrees incidence angle.
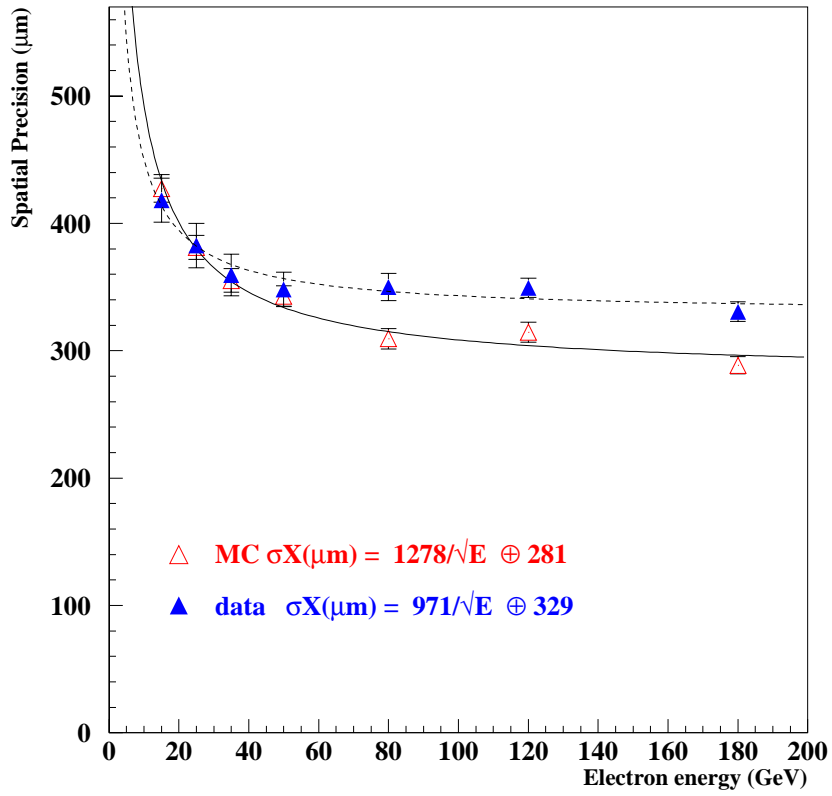
Figure 29: Spatial precision as a function of electron energy for the first plane, twenty degrees incidence angle.
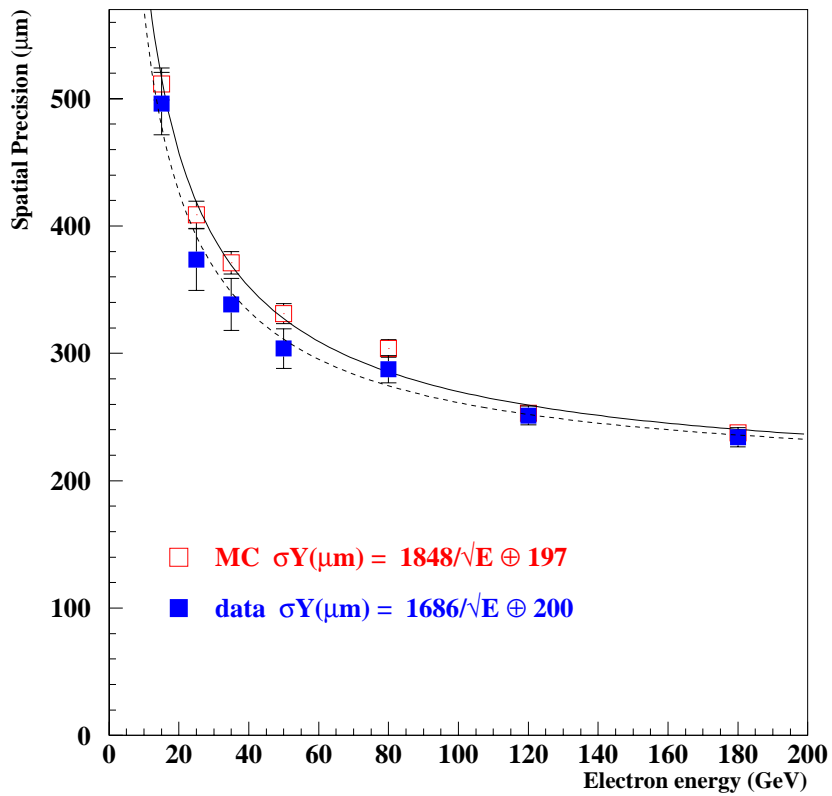

Figure 30: Spatial precision as a function of electron energy for the second plane, twenty degrees incidence angle.

5 Beam Test 2000

The preshower prototype has a total of 3.24 X_0 which is thicker than forseen in CMS [4]. It is planned to reduce this thickness to something more realistic for beam tests in 2000. The accuracy of the simulation allows us to predict the effects on the energy resolution etc. of modifying the preshower geometry. Two scenarios were studied, each involving the removal of material from the steel support plates, to obtain total preshower thicknesses (for normally incident particles) of about 3.0 X_0 and 2.8 X_0.

Figure 31 shows the energy resolution for these "thinner" scenarios at 25, 50 and 120 GeV, compared with the 3.2 X_0 geometry. Also shown is a curve representing the TDR design goal. The preshower additional term decreases from 0.55% to 0.43% at 120 GeV.
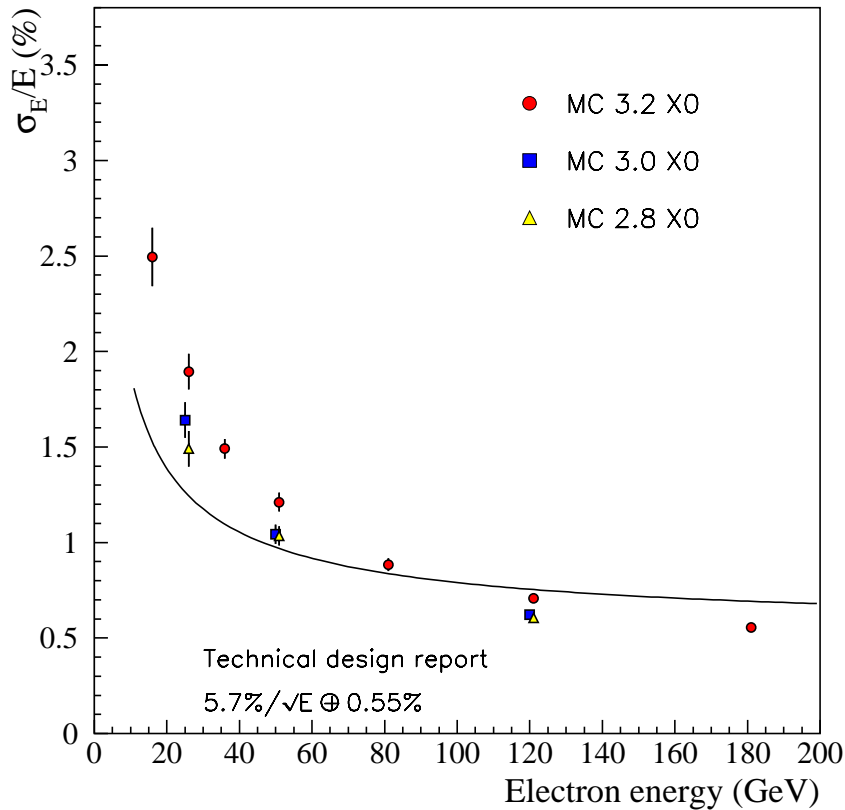

Figure 31: Energy resolution with preshower thicknesses of 3.24 X_0, 3.0 X_0 and 2.8 X_0. Note that noise is not included.

The preshower and ECAL prototype will be placed in a 3T magnetic field (in the endcap configuration) in the H2 beam line at CERN in 2000. The simulation predicts that the effects of this field on the performance of the preshower are negligible.

6 Conclusions

The excellent agreement between data and simulation now gives us confidence that we can use simulation to predict the effects of design changes etc. on the preshower performance - both the prototype and the "real" detector.

The energy resolution results obtained are encouraging, particularly as it was impractical to use an array of crystals larger than 3x3 in the E_{tot} calculation due to noise constraints and the total thickness of the preshower was significantly larger than it will be in CMS. Above about 80 GeV (equivalent to an E_T of less than 35 GeV in the endcaps of CMS) the energy resolution is better than 1%. The spatial precision obtained is easily sufficient for our requirements.

The short time needed for installation in the beam resulted in efficient and complete data taking and the system ran continuously for the complete period of about 150 hours without any user intervention.

Acknowledgments

We wish to thank all those involved in the construction and operation of the Endcap ECAL matrix used in this test, particularly Dave Cockerill for agreeing to our wishes to push the supercrystal as far forward as possible, and to Geoff Barber for making this physically possible. Chris Seez and Maurice Haguenauer were, as usual, extremely helpful in many areas of both software and hardware.

References

[1] P. Aspell, *The design of the PACE integrated circuit for the LHC CMS Preshower Detector System*, Open University T401 report - see http://cmsdoc.cern.ch/~pshower/documents/internal/pacethesis.pdf

[2] Note in preparation

[3] P. Bloch, *Getting the best resolution from the H4 beam chambers*, CMS IN-1996/006

[4] The CMS Collaboration, *The Electromagnetic Calorimeter Project - Technical Design Report*, CERN/LHCC 97-33